Author/s:
Lv, C-K;Zheng, F;Yang, X-Y;Bi, P-Q;Niu, M-S;Wang, Y-Z;Smith, TA;Ghiggino, KP;Hao, X-T

Title:
Optimizing the Crystallinity and Phase Separation of PTB7:PC71BM Films by Modified Graphene Oxide

Date:
2018-02-08

Citation:
Lv, C. -K., Zheng, F., Yang, X. -Y., Bi, P. -Q., Niu, M. -S., Wang, Y. -Z., Smith, T. A., Ghiggino, K. P. & Hao, X. -T. (2018). Optimizing the Crystallinity and Phase Separation of PTB7:PC71BM Films by Modified Graphene Oxide. The Journal of Physical Chemistry C, 122 (5), pp.2572-2581. https://doi.org/10.1021/acs.jpcc.7b11726.

Optimizing the Crystallinity and Phase Separation of PTB7:$PC_{71}BM$ Films by Modified Graphene Oxide

Cheng-Kun Lv,[†] Fei Zheng,[†] Xiao-Yu Yang,[†] Peng-Qing Bi,[†] Meng-Si Niu,[†] Yu-Zhu Wang,*[,‡] Trevor A. Smith,[§] Kenneth P. Ghiggino,[§] Xiao-Tao Hao*[,†,§]

[†]*School of Physics, State Key Lab of Crystal Materials, Shandong University, Jinan 250100, China*

[‡]*Shanghai Synchrotron Radiation Facility, Shanghai Institute of Applied Physics, Chinese Academy of Sciences, Shanghai 200240, China*

[§]*ARC Centre of Excellence in Exciton Science, School of Chemistry, The University of Melbourne, Parkville, Victoria 3010, Australia*

ABSTRACT: A facile method is proposed to obtain modified shorn graphene oxide (DDAB-sGO) with improved dispersion in organic solvents. DDAB-sGO, which exhibits good dispersibility in the non-polar solvent o-dichlorobenzene (DCB), was obtained via the sono-Fenton reaction and didodecyl dimethyl ammonium bromide (DDAB) ionic functionalization. DDAB-sGO was used in the preparation of conjugated polymer:fullerene blend composites. UV-visible absorption spectra, steady-state photoluminescence spectra, fluorescence decay and grazing incidence X-ray scattering measurements were applied to characterize morphologies, structural features and charge transport characteristics of the composites. Doped into poly[[4,8-bis[(2-ethylhexyl) oxy] benzo[1,2-b:4,5-b'] dithiophene-2,6-diyl] [3-fluoro-2-[(2-ethylhexyl) carbonyl] thieno [3,4-b] thiophenediyl]] (PTB7):[6,6]-phenyl C_{71} butyric acid methyl ester ($PC_{71}BM$) conjugated polymer blends, DDAB-sGO is shown to facilitate increased crystallinity and phase separation of PTB7 and $PC_{71}BM$ to achieve a more optimal morphology for bulk heterojunction solar cells (PSCs) resulting in a ~12% enhancement in power conversion efficiency (PCE) over the undoped PTB7:$PC_{71}BM$ blend.

INTRODUCTION

Graphene oxide (GO) is a layer-structured nonstoichiometric material obtained by an improved Hummers' method from graphite.[1] Recently, GO has attracted considerable attention in the fields of microelectronics, biosensors and organic optoelectronics,[2-6] mainly due to its superior properties, i.e. low cost, flexibility and large specific surface area, high dispersibility in water and adjustable band gap.[7] The incorporation of GO with conjugated polymers to change the polymer films' structure and charge transport characteristics is an effective way to obtain enhanced performance of organic optoelectronic devices.[8-11] The structure of GO is a graphene sheet bonded with oxygen-containing groups, which allows GO to be used as a stably dispersed monolayer in water and other solvents. More specifically, GO has epoxy and hydroxyl groups in its basal plane and carbonyl and carboxyl groups on its edge.[12] In 2011, Rourke et al. proposed a novel structural model of GO, in which oxidative debris was adsorbed on large alkali-washed GO surfaces by π-π stacking.[13] However, the hydrophilic nature and large surface area of GO have side effects relating to its dispersion into nonpolar solvents, by contrast forming irreversible aggregation,[14] thus blocking its path in the synthesis of GO/polymer composites. Functionalized modification of GO can not only improve GO dispersion in nonpolar organic solvents, but also expand the scope of applications of functionalized GO.[15] There are several methods for the functionalization of GO broadly divided into covalent and noncovalent bond modification, with the latter further divided into ionic bonding,[16] intermolecular π-π stacking,[17] hydrogen bond modification.[2] Our team has previously reported a facile method to synthesize the cationic surfactant DDAB functionalized GO (DDAB-GO) and further synthesized 2-chlorophenyl isocyanate (CI)-DDAB-GO

by CI treatment, which improved GO dispersion and compatibility with a conjugated polymer in nonpolar solvents, and supported the oxidative debris model.[18-20]

In this work, we have prepared small graphene oxide (sGO) sheets based on the sono-Fenton reaction and ethanol as the intermedium, then successfully transferred it from water to the nonpolar solvent, dichlorobenzene (DCB) forming stable dispersions. With the help of a cationic surfactant, didodecyl dimethyl ammonium bromide (DDAB), the DDAB functionalized shorn GO (DDAB-sGO) was obtained, which has improved compatibility with a conjugated polymer. DDAB-sGO was added into poly[[4,8-bis[(2-ethylhexyl) oxy] benzo[1,2-b:4,5-b'] dithiophene-2,6-diyl] [3-fluoro-2-[(2-ethylhexyl) carbonyl] thieno [3,4-b] thiophenediyl]:[6,6]-phenyl C_{71} butyric acid methyl ester (PTB7: $PC_{71}BM$) conjugated polymer blends to improve the crystallinity and charge transport properties, resulting in an enhancement of the power conversion efficiency (PCE) of bulk heterojunction (BHJ) polymer solar cells (PSCs).

EXPERIMENTAL SECTION

Materials. The graphene oxide powder, which was claimed to be synthesized by an improved Hummer's method, was purchased from XFNANO Materials Technologic Co. Ltd. (Nanjing, China). Didodecyl dimethyl ammonium bromide (DDAB) and o-dichlorobenzene (DCB) were supplied from Aladdin Corporation (Shanghai, China). PTB7 and $PC_{71}BM$ were purchased from Solarmer Materials, Inc. (Beijing, China). 1,8-diodooctane (DIO) and iron(III) chloride ($FeCl_3$) powder were purchased from Sigma-Aldrich Corporation (USA). Dialysis tubing (3500D) purchased from Yuanye Biological Technology Co. Ltd. (Shanghai, China) was rinsed with deionized (DI) water while other materials mentioned above were used as received.

Prefabrication of sGO and DDAB-sGO. The sono-Fenton reaction was modified

to easily synthesize the small graphene oxide (sGO) sheets.[21] 10 ml H_2O_2 (30% wt.) was added to 50 ml 0.5 mg/ml GO solution followed by magnetic bar stirring. Sodium hydroxide (NaOH) solution was added dropwise to the mixed solution to adjust the solution pH to ~ 7. After 2.5 ml $FeCl_3$ (2 mg/ml) was added with continuous stirring for 30 minutes, the solution was kept in an ultrasonic (200 W) water bath for at least four hours. The reaction products were dialyzed for 2 days to remove iron ions to obtain a 0.4mg/ml sGO solution.

8 ml DDAB/(water/alcohol) (1:1) solution (1 mg/ml) was added to 10 ml 0.4 mg/ml sGO solution and the mixture was shaken for several minutes to accomplish the ionic functionalization process. Small brown particles appeared and then 4 ml DCB was added followed by stirring for six hours. After resting until the clear phase separation appeared (~12 hours), 1 mg/ml DDAB-sGO/DCB solution was obtained after the upper transparent layer was removed. 4 ml anhydrous ethanol was added with water-bath ultrasonic treatment (200W) for 5 minutes, and then 4 ml DI water was added and the solution stirred for 4 hours. The transparent upper-layer solution was removed after 2 hours. The purification process was repeated at least three times to obtain high purity DDAB-sGO/DCB with a concentration of ~1 mg/ml.

Photophysical Characterization. Transmission Electron Microscope (TEM) images were taken using a JEM-100CX II TEM (JEOL). The Atomic Force Microscopy(AFM) images were obtained using the tapping mode of a Multimode Scanning Probe Microscope (NanoScope-IIIA, Veeco Metrology Group). Fourier Transform Infrared (FTIR) spectroscopy was performed on KBr wafer substrates and recorded under the single channel mode of the FTIR Spectrometer (Vertex-70, Bruker, Co.). The UV-vis absorbance and the steady-state photoluminescence (PL) spectra were recorded on either a UV-visible dual-beam spectrophotometer (TU-1900, PG

Instruments Co., Ltd.) or a fiber optic spectrometer (PG2000 Pro, Idea Optics Co., Ltd.). The excitation laser was the output of a frequency doubled femtosecond Ti-sapphire laser (Maitai HP, Spectra-Physics) at 80 MHz. Time-resolved photoluminescence (TRPL) decay profiles and 2D time-resolved fluorescence images were obtained by confocal optical microscopy (Nanofinder FLEX2. Tokyo Instruments, Inc.) combined with a time-correlated single-photon counting (TCSPC) module (Becker & Hickl, SPC-150, ANDOR DU420A-OE, excitation wavelength at 500 nm, detection wavelength at 725 nm).

Grazing Incidence X-ray Scattering (GIXS) Measurements. The active layer solution was spin-coated on the Si wafers to prepare samples for Grazing Incidence X-ray Scattering (GIXS) measurements. Both wide angle and small angle GIXS (GIWAXS and GISAXS) measurements of samples were recorded at the Shanghai Synchrotron Radiation Facility (SSRF). The photon wavelength of the BL16B1 beamline is 0.124 nm. The scattering intensities of samples were measured by a CCD detector (MAR-165) with a pixel size of 80 μm. The 2D-GISAXS measurements were carried out by setting the incidence angle of the X-ray beam to be 0.12° and the sample-detector distance to be 2500 mm, the 2D-GIWAXS measurements data were typically collected for 200 s when the incidence angle was 0.3 ° and the sample-detector distance was 200 mm. The 1-D data were analyzed by the software Q2d and the 2-D image analysis was exported by the software Fit2d.

Fabrication and Characterization of Organic Solar Cells. The PTB7:$PC_{71}BM$ (1:1.7)[22] composite (27 mg/ml) was dissolved in DCB and DIO (97:3), then mixed with 1mg/ml DDAB-sGO solution for characterization purposes and solar cell devices. The PSCs were fabricated with an inverted sandwich structure of ITO/ZnO (40 nm)/active layer (100nm)/MoO_3 (7.5 nm)/Ag (100 nm). The ITO substrates (sheet

resistance 15 Ω·square^{-1}) were prepatterned on glass by the manufacturer and cleaned sequentially with detergent, deionized water, acetone, absolute ethyl alcohol, and isopropanol in an ultrasonic treatment for 20 minutes each time. The electron transport layer (ZnO) and active layer were spin-coated in a N_2 filled glove box.[23] The hole transporting layer (MoO_3) and anode electrodes (Ag) were then deposited by thermal evaporation in a vacuum cavity with a base pressure < 1.5 × 10 $^{-6}$ Torr at the evaporation rate of 1.2 and 0.3 Å/s, respectively. Each organic solar cell has the same effective area of 2x2 mm. The current density-voltage (J−V) characteristics of the devices were measured by a programmable voltage−current sourcemeter (2400, Keithley Instruments Inc., Cleveland, OH, U.S.A.) under AM 1.5G illumination of 100 mW/cm^2 provided by a Xenon lamp solar simulator (Sofn Instruments Co., Ltd. China). The charge carrier mobilities were measured from the hole-only devices and electron-only devices in the dark and extracted by the space charge limited current (SCLC) model.[24-30] The external quantum efficiency (EQE) profiles of the devices were measured by a QEX10 system (PV Measurement, Inc.) in air at room temperature.

RESULTS AND DISCUSSION

Figure 1a presents the molecular structures of GO and DDAB, while **Figure 1**b illustrates the reaction pathway from GO to DDAB-sGO. Large-dimension (micrometer size) GO was disintegrated into small GO particles (sGO) through the sono-Fenton reaction. The DDAB cations with two long alkyl chains (hydrophobic groups) are mainly attached to the ionized carboxylic anions at the edge of the sGO sheets through ionic bonds during the functionalization procedure with DDAB. With the help of ethanol as a medium, the transfer of DDAB-sGO from water to DCB can

be further achieved.[18,31,32]

AFM images of sGO and DDAB-sGO films are shown in **Figure 2**a,b. The height profiles corresponding to the red lines are shown in **Figure 2**c,d indicating that both sGO and DDAB-sGO sheets are predominantly mono-layered with a thickness of approximately 1~2 nm.[33] The thickness of DDAB-sGO (~1.8 nm) is larger than that of sGO (1.2 nm), indicating the grafting of chemical groups to the basal plane of sGO sheets after DDAB treatment. In addition, **Figure 2**a shows that the phase size of sGO is quite mixed after the sono-Fenton reaction. Once sGO was ionically functionalized by DDAB, the phase size of DDAB-sGO (shown in **Figure 2**d) is similar (~24 nm) but more uniform, which is consistent with the TEM image (insert in **Figure 2**b) and indicates the DDAB ion functionalization selected the sGO sheets with similar phase size.

The main absorption band in the UV-vis absorption spectra (**Figure 2**e) of GO, sGO and DDAB-sGO films, is attributed to the π–π transition of the C=C bond and has a peak at 226 nm for GO.[34] From GO to DDAB-sGO, the absorption peak at approximately 300 nm, corresponding to the n–π transition of C=O, almost disappears while the π–π transition peak position obviously blue-shifts to below 200 nm, which both indicate the diminution of sp^2 conjugation domains. The FTIR spectra of DDAB-GO (**Figure 2**f) have characteristic bands at 1732 cm^{-1} corresponding to the >C=O stretching mode from the carboxyl and carbonyl groups of GO and at 1611 cm^{-1} corresponding to the C=C stretching mode from the π–π stacking. The FTIR spectrum of DDAB-sGO exhibits band maxima at 1736 cm^{-1} and 1644 cm^{-1} that are less apparent than the corresponding bands in DDAB-GO because of the decreased domain size. The band peak observed at 1611 cm^{-1} of DDAB-sGO shifts to 1644 cm^{-1}, which is also attributed to the decreased conjugate phase size in DDAB-sGO.[21]

PTB7 is a well-known conjugated polymer with good electrical and optical properties that has been widely used in organic electronics.[35] DDAB-sGO was added into the PTB7:$PC_{71}BM$ system to explore its impact on photophysical behavior and potential for photovoltaic applications. The optical microscopy images of PTB7:$PC_{71}BM$ and PTB7:$PC_{71}BM$:1% DDAB-sGO blend films are shown in **Figure 3**a,b, respectively. The surface morphology of PTB7:$PC_{71}BM$:1% DDAB-sGO is comparable to that of pure PTB7:$PC_{71}BM$ films except for several dark spots attributed to $PC_{71}BM$ aggregates. The changes (characterized by AFM) in surface film morphology before/after DDAB-sGO incorporation are shown in **Figure 3**c,d, respectively. The R_q (the root mean square of the roughness) is 2.95 nm for PTB7: $PC_{71}BM$ and 3.08 nm for PTB7: $PC_{71}BM$: 1% DDAB-sGO films, revealing a slightly increased roughness induced by the addition of the DDAB-sGO. The incorporation of DDAB-sGO not only has little detrimental effect on the morphology of conjugated polymer films, but also promotes $PC_{71}BM$ aggregation, which is often beneficial to charge transport.

The absorbance and molecular interactions of composites in PTB7:$PC_{71}BM$ films with/without DDAB-sGO incorporation are identified through UV-vis absorption (shown in **Figure 3**e,f). The UV-vis absorption spectra (**Figure 3**e) show clearly enhanced absorbance attributed to DDAB-sGO in the PTB7:$PC_{71}BM$ conjugation blend films with the same thickness. The enhanced interchain interaction is sensitive to the improved CT state at the donor/accepter interface and the charge carriers' transport progress. Previously, Spano et al. reported that the interchain coupling and the degree of structural order can be reflected in the absorption ratio[36,37] of two peaks (shown in **Figure 3**f), whose intensities are denoted I_{0-0} and I_{0-1}, which are attributed to the transitions between the ground state and the first two vibronic levels of the

excited state.[38-40] The spectra, normalized at the 0−1 transition peak intensity to simplify the comparison of the relative 0-0 peak intensities, are shown in **Figure 3**f and can be used to evaluate the intrachain interactions of PTB7:$PC_{71}BM$ blend films.[40,41] The magnitude of the I_{0-0}/I_{0-1} ratio reflecting the size of the aggregate for PTB7:$PC_{71}BM$:1% DDAB-sGO film is obviously higher than that for pristine PTB7:$PC_{71}BM$ film, while the 0-0 peak red-shifts slightly from 682 nm to 685 nm. We assume that this behavior is due to an increase in the size of the aggregates in the PTB7:$PC_{71}BM$ blend films. The numerous sp^2 conjugation domains in DDAB-sGO sheets provide an ideal platform for assembling polymer chains via π-π stacking,[42] which explains increased interchain interactions and a higher crystalline content of PTB7 induced by DDAB-sGO.

The time-resolved fluorescence images (detection wavelength at 725nm) for PTB7:$PC_{71}BM$ and PTB7:$PC_{71}BM$:1% DDAB-sGO blend films are shown in **Figure 4**a,b, respectively. The corresponding average fluorescence lifetime distribution histograms extracted from the lifetime images are shown in **Figure 4**c. The average lifetimes of the PTB7:$PC_{71}BM$ film are centered around 42-53 ps with a peak at 47 ps, while the distribution is in the range of 34-45 ps with the peak shifted to ~39 ps when DDAB-sGO was incorporated. This reduction in the average emission decay time indicates that the presence of DDAB-sGO can promote rapid exciton dissociation at the donor/acceptor interface.[43] Fluorescence decay curves[44] (**Figure 4**d), corresponding to marked regions within the two images, confirm that the fluorescence of the PTB7:$PC_{71}BM$ film decays more rapidly with the incorporation of DDAB-sGO. The parameters fitted by fitting a double exponential decay function are presented in **Table 1**. The reduced average fluorescence decay time of the PTB7:$PC_{71}BM$:1% DDAB-sGO blend film is partly attributed to the optimized morphology, which

provides more donor/acceptor interface area for photo-excitons dissociation. And in our previous work, we have measured the energy level of DDAB functionalized GO by cyclic voltammograms (CV) method, whose LUMO is -3.6 eV and lower than that of PTB7 (-3.3 eV).[20] Therefore, it is also partly attributed to electron transfer from photo-excited PTB7 to DDAB-sGO. These results suggest the possible applications of the addition of small DDAB-sGO in polymer optoelectronic devices for electron collection and transportation.[45,46]

The 2-D GIWAXS spectra are used to investigate the crystallinity and molecular orientation of these composite films systematically.[47] In **Figure 5**a,b, pronounced out-of-plane arc-like scattering peaks (100) arising from the Bragg diffraction of periodic PTB7 lamellae are observed at q = 2-3 nm^{-1}, and small reflection peaks (010) are observed at q = 14-16 nm^{-1}. The scattering intensity of the (100) peaks increased significantly after adding DDAB-sGO, suggesting this addition enhanced the molecular stacking and crystallinity of the PTB7 copolymers. The small reflection peaks (010) show little obvious change upon the addition of DDAB-sGO. The spectra of the polymer:PCBM blend films (**Figure 5**c,d**)** also exhibit an enhanced scattering peak at q =13-14 nm^{-1} corresponding to the Bragg diffraction of $PC_{71}BM$. The incorporation of small DDAB-sGO leads to not only increased local ordering and crystallinity but also larger phase separated domain sizes of both PTB7 and $PC_{71}BM$, which improves the charge transfer and collection efficiency of PSCs.

Figure 6 shows the 2-D GISAXS images which provide quantitative information of domain size and the corresponding integrated profiles along the q_{xy} direction in PTB7:$PC_{71}BM$ films.[48] The reinforced scattering in the low-q region (shown in **Figure 6**a,b) is attributed to $PC_{71}BM$ aggregates caused by the improved phase separation in the PTB7:$PC_{71}BM$ system.[49,50] To obtain detailed structural information

of $PC_{71}BM$ aggregates, the Guinier approximation was applied to calculate the radius of gyration (Rg) of a $PC_{71}BM$ cluster:

$$ln\,(I(q)) = ln\big(I(0)\big) - \frac{R^2}{3}q^2 \qquad (1)$$

where q is the coordinate along the projection direction, *I(q)* is the scattering intensity and R is the radius of $PC_{71}BM$ clusters.[51] The value of R is obtained by taking the slope of the linear correlation between *ln(I(q))* and q^2 using **Equation (1)**. Two fitting lines are used to decrease experimental error. After the incorporation of 1% DDAB-sGO, the average radius of $PC_{71}BM$ domains increases slightly from 24.25 nm to 27.67 nm. Combined with the results of the AFM image (**Figure 3**d), it is the evident that the incorporation of DDAB-sGO induces more PTB7 molecules to be expelled away from the $PC_{71}BM$ clusters. It explains an increased phase size and crystallinity of $PC_{71}BM$, which may improve the electron mobility. Increased phase size of PTB7 and $PC_{71}BM$ allows a larger phase separation of PTB7 and PCBM but optimized surface morphology.

The energy-level diagram for the individual components of inverted BHJ PSCs[52,53] based on PTB7:$PC_{71}BM$ blend films are depicted in **Figure 7**a. **Figure 7**b shows the dark current characteristic curves from hole-only and electron-only devices corrected by $V\text{-}V_{bi}$, which indicates the charge carrier mobilities calculated from the SCLC measurement. The hole and electron mobilities are extracted using the Mott-Gurney law:

$$J = \frac{9}{8}\varepsilon\varepsilon_0\mu\frac{V^2}{d^3} \qquad (2)$$

where ε_0 is the vacuum dielectric constant of 8.85×10^{-12} F/m, ε is the relative permittivity of the polymer film (assumed as 3),[29,30,54-56] d is the thickness of sample films and μ is the charge carrier mobility summarized in **Table 2**. Compared with the

control group devices, the hole mobility of devices with DDAB-sGO added is raised from 1.23×10^{-4} $cm^2V^{-1}s^{-1}$ to 2.63×10^{-4} $cm^2V^{-1}s^{-1}$, while the electron mobility is raised from 2.14×10^{-4} $cm^2V^{-1}s^{-1}$ to 4.19×10^{-4} $cm^2V^{-1}s^{-1}$. With the incorporation of DDAB-sGO, the improved crystallinity of both PTB7 and $PC_{71}BM$ can raise the charge mobility and further promote more balanced charge carrier transport in the vertical direction, while the optimized phase separation of PTB7 and $PC_{71}BM$ can facilitate the exciton diffusion to polymer/fullerene interfaces, both of which can decrease the current loss and increase the J_{sc} of OSCs.[57,58] The current density-voltage curves and EQE of PSCs with the best PCE are shown in **Figure 7**c,d, while the device performance parameters including the average and best values of short-circuit current density (J_{sc}) , open-circuit voltage (V_{oc}), fill factor (FF), PCE are summarized in **Table 2**.[59] After adding DDAB-sGO, the J_{sc} increases markedly from 14.1 to 15.8 mA/cm^2 and the FF increases slightly from 67 to 68%, enhancing the PCE by ~12% (from 7.05% to 7.9%). The significant performance improvement of PSCs is attributed to the enhanced light absorption (confirmed by EQE) and improved phase separation of PTB7 and $PC_{71}BM$ with an optimized morphology induced by the small DDAB-sGO sheets.

CONCLUSIONS

We have demonstrated a facile and effective route for synthesizing small-sized and functionalized graphene oxide (DDAB-sGO) sheet dispersions in a nonpolar solvent, which is based on the sono-Fenton reaction and DDAB ionic functionalization. The presence of DDAB-sGO is suggested to facilitate increased crystallinity and phase separation of PTB7 and $PC_{71}BM$ and further enhance the charge transport and collection efficiency, leading to an improved performance of organic solar cells by

~12% PCE.

AUTHOR INFORMATION

Corresponding Authors

*Email: haoxt@sdu.edu.cn. (X.-T. Hao)

*Email: wangyuzhu@sinap.ac.cn. (Y.-Z. Wang)

Notes

The authors declare no competing financial interest.

ACKNOWLEDGEMENTS

This work was supported by the National Natural Science Foundation of China (No. 11574181, 61631166001); the Fundamental Research Funds of Shandong University (2015JC047); Open Research Fund of State Key Laboratory of Polymer Physics and Chemistry, Changchun Institute of Applied Chemistry, Chinese Academy of Sciences (2015014), the "National Young 1000 Talents" Program of China. Support from the University of Melbourne International Research and Research Training Fund (IRRTF) and the ARC Centre of Excellence in Exciton Science (CE170100026) are acknowledged. The authors would like to thank the Shanghai Synchrotron Radiation Facility (beamline BL16B1) for providing the beam time for GIXS measurements.

REFERENCES

(1) Stankovich, S.; Piner, R. D.; Chen, X.; Wu, N.; Nguyen, S. B. T.; Ruoff, R. S. Stable Aqueous Dispersions of Graphitic Nanoplatelets via the Reduction of Exfoliated Graphite Oxide in the Presence of Poly(sodium 4-styrenesulfonate). *J. Mater. Chem.* **2006**, *16*, 155-158.

(2) Georgakilas, V.; Tiwari, J. N.; Kemp, K. C.; Perman, J. A.; Bourlinos, A. B.; Kim, K. S.; Zboril, R. Noncovalent Functionalization of Graphene and Graphene Oxide for Energy Materials, Biosensing, Catalytic, and Biomedical Applications. *Chem. Rev.* **2016**, *116*, 5464-5519.

(3) Li, P.; Stasio, F. D.; Eda, G.; Fenwick, O.; Mcdonnell, S. O.; Anderson, H. L.; Chhowalla, M.; Cacialli, F. Luminescent Properties of a Water−Soluble Conjugated Polymer Incorporating Graphene−Oxide Quantum Dots. *ChemPhysChem* **2015**, *16*, 1258-1262.

(4) Wang, H.; Robinson, J. T.; Li, X.; Dai, H. Solvothermal Reduction of Chemically Exfoliated Graphene Sheets. *J. Am. Chem. Soc.* **2009**, *131*, 9910-9911.

(5) Zhu, Y.; Stoller, M. D.; Cai, W.; Velamakanni, A.; Piner, R. D.; Chen, D.; Ruoff, R. S. Exfoliation of Graphite Oxide in Propylene Carbonate and Thermal Reduction of the Resulting Graphene Oxide Platelets. *ACS Nano* **2010**, *4*, 1227-1233.

(6) Samulski, T. D.; Si, G. Y. Synthesis of Water Soluble Graphene. *Nano Lett.* **2008**, *8*, 1679–1682.

(7) Iwase, A.; Yun, H. N.; Ishiguro, Y.; Kudo, A.; Amal, R. Reduced Graphene Oxide as a Solid-State Electron Mediator in Z-Scheme Photocatalytic Water Splitting under Visible Light. *J. Am. Chem. Soc.* **2011**, *133*, 11054-11057.

(8) Chao, Y. H.; Wu, J. S.; Wu, C. E.; Jheng, J. F.; Wang, C. L.; Hsu, C. S. Solution-Processed (Graphene Oxide)-(d^0Transition Metal Oxide) Composite Anodic Buffer Layers toward High-Performance and Durable Inverted Polymer Solar Cells. *Adv. Energy Mater.* **2013**, *3*, 1279-1285.

(9) Li, S. S.; Tu, K. H.; Lin, C. C.; Chen, C. W.; Chhowalla, M. Solution-Processable Graphene Oxide as an Efficient Hole Transport Layer in Polymer Solar Cells. *ACS Nano* **2010**, *4*, 3169-3174.

(10) Hocker, S.; Hudson-Smith, N.; Schniepp, H. C.; Kranbuehl, D. E. Enhancing Polyimide's Water Barrier Properties through Addition of Functionalized Graphene Oxide. *Polymer* **2016**, *93*, 23-29.

(11) Kim, H.; Miura, Y.; Macosko, C. W. Graphene/Polyurethane Nanocomposites for Improved Gas Barrier and Electrical Conductivity. *Chem. Mater.* **2010**, *22*, 3441-3450.

(12) He, H.; Klinowski, J.; Forster, M.; Lerf, A. A New Structural Model for Graphite Oxide. *Chem. Phys. Lett.* **1998**, *287*, 53-56.

(13) Rourke, J. P.; Pandey, P. A.; Moore, J. J.; Bates, M.; Kinloch, I. A.; Young, R. J.; Wilson, N. R. The Real Graphene Oxide Revealed: Stripping the Oxidative Debris from the Graphene−like Sheets. *Angew. Chem. Int. Ed. Engl.* **2011**, *50*, 3173-3177.

(14) Niyogi, S.; Bekyarova, E.; Itkis, M. E.; Mcwilliams, J. L.; Hamon, M. A.; Haddon, R. C. Solution Properties of Graphite and Graphene. *J. Am. Chem. Soc.* **2006**, *128*, 7720-7721.

(15) Georgakilas, V.; Otyepka, M.; Bourlinos, A. B.; Chandra, V.; Kim, N.; Kemp, K. C.; Hobza, P.; Zboril, R.; Kim, K. S. Functionalization of Graphene: Covalent and Non-covalent Approaches, Derivatives and Applications. *Chem. Rev.* **2012**, *112*, 6156-6214.

(16) Chen, D.; Feng, H.; Li, J. Graphene Oxide: Preparation, Functionalization, and

Electrochemical Applications. *Chem. Rev.* **2012**, *112*, 6027-6053.

(17) Qu, Y.; Su, Q.; Li, S.; Lu, G.; Zhou, X.; Zhang, J.; Chen, Z.; Yang, X. H-Aggregated Form II Spherulite of Poly(3-butylthiophene) Grown from Solution. *ACS Macro Lett.* **2012**, *1*, 1274-1278.

(18) Zheng, F.; Xu, W. L.; Jin, H. D.; Zhu, M. Q.; Yuan, W. H.; Hao, X. T.; Ghiggino, K. P. Purified Dispersions of Graphene in a Nonpolar Solvent via Solvothermal Reduction of Graphene Oxide. *Chem. Commun.* **2015**, *51*, 3824-3827.

(19) Zheng, F.; Yang, X. Y.; Bi, P. Q.; Niu, M. S.; Lv, C. K.; Feng, L.; Hao, X. T.; Ghiggino, K. P. Improved Compatibility of DDAB-functionalized Graphene Oxide with a Conjugated Polymer by Isocyanate Treatment. *RSC Adv.* **2017**, *7*, 17633-17639.

(20) Zheng, F.; Xu, W. L.; Jin, H. D.; Hao, X. T.; Ghiggino, K. P. Charge Transfer from Poly (3-hexylthiophene) to Graphene Oxide and Reduced Graphene Oxide. *RSC Adv.* **2015**, *5*, 89515-89520.

(21) Routh, P.; Das, S.; Shit, A.; Bairi, P.; Das, P.; Nandi, A. K. Graphene Quantum Dots from a Facile Sono-Fenton Reaction and its Hybrid with a Polythiophene Graft Copolymer Toward Photovoltaic Application. *ACS Appl. Mater. Inter.* **2013**, *5*, 12672–12680.

(22) Kong, J.; Hwang, I. W.; Lee, K. Top-down Approach for Nanophase Reconstruction in Bulk Heterojunction Solar Cells. *Adv. Mater.* **2014**, *26*, 6275-6283.

(23) Sun, Y.; Seo, J. H.; Takacs, C. J.; Seifter, J.; Heeger, A. J. Inverted Polymer Solar Cells Integrated with a Low−Tamperature−Annealed Sol−Gel−Derived ZnO Film as

an Electron Transport Layer. *Adv. Mater.* **2011**, *23*, 1679-1683.

(24) Melzer, C.; Koop, E. J.; Mihailetchi, V. D.; Blom, P. W. M. Hole Transport in Poly(phenylene vinylene)/Methanofullerene Bulk-Heterojunction Solar Cells. *Adv. Funct. Mater.* **2004**, *14*, 865-870.

(25) Foster, S.; Deledalle, F.; Mitani, A.; Kimura, T.; Kim, K.-B.; Okachi, T.; Kirchartz, T.; Oguma, J.; Miyake, K.; et al. Electron Collection as a Limit to Polymer:PCBM Solar Cell Efficiency: Effect of Blend Microstructure on Carrier Mobility and Device Performance in PTB7:PCBM. *Adv. Energy Mater.* **2014**, *4*, 1400311-1400315.

(26) Saeki, H.; Kurimoto, O.; Nakaoka, H.; Misaki, M.; Kuzuhara, D.; Yamada, H.; Ishida, K.; Ueda, Y. Effect of Crystallinity in Small Molecular Weight Organic Heterojunction Solar Cells. *J. Phys. Chem. C* **2014**, *2*, 5357-5364.

(27) Zheng, Y.; Goh, T.; Fan, P.; Shi, W.; Yu, J.; Taylor, A. D. Toward Efficient Thick Active PTB7 Photovoltaic Layers Using Diphenyl Ether as a Solvent Additive. *ACS Appl. Mater. Inter.* **2016**, *8*, 15724-15731.

(28) Wang, H.; Huang, J.; Xing, S.; Yu, J. Improved Mobility and Lifetime of Carrier for Highly Efficient Ternary Polymer Solar Cells Based on TIPS-pentacene in PTB7: PC71BM. *Org. Electron.* **2016**, *28*, 11-19.

(29) Ebenhoch, B.; Thomson, S. A. J.; Genevičius, K.; Juška, G.; Samuel, I. D. W. Charge Carrier Mobility of the Organic Photovoltaic Materials PTB7 and $PC_{71}BM$ and its Influence on Device Performance. *Org. Electron.* **2015**, *22*, 62-68.

(30) Shrotriya, V.; Yao, Y.; Li, G.; Yang, Y. Effect of Self-Organization in Polymer/Fullerene Bulk Heterojunctions on Solar Cell Performance. *Appl. Phys. Lett.*

2006, *89*, 063505.

(31) Paredes, J. I.; Villar-Rodil, S.; Martínez-Alonso, A.; Tascón, J. M. D. Graphene Oxide Dispersions in Organic Solvents. *Langmuir* **2008**, *24*, 10560-10564.

(32) Liang, Y.; Wu, D.; Feng, X.; Müllen, K. Dispersion of Graphene Sheets in Organic Solvent Supported by Ionic Interactions. *Adv. Mater.* **2009**, *21*, 1679-1683.

(33) Marcano, D. C.; Kosynkin, D. V.; Berlin, J. M.; Sinitskii, A.; Sun, Z.; Slesarev, A.; Alemany, L. B.; Lu, W.; Tour, J. M. Improved Synthesis of Graphene Oxide. *ACS Nano* **2010**, *4*, 4806-4814.

(34) Eda, G.; Lin, Y. Y.; Mattevi, C.; Yamaguchi, H.; Chen, H. A.; Chen, I. S.; Chen, C. W.; Chhowalla, M. Blue Photoluminescence from Chemically Derived Graphene Oxide. *Adv. Mater.* **2010**, *22*, 505-509.

(35) Hedley, G. J.; Ward, A. J.; Alekseev, A.; Howells, C. T.; Martins, E. R.; Serrano, L. A.; Cooke, G.; Ruseckas, A.; Samuel, I. D. Determining the Optimum Morphology in High-Performance Polymer-Fullerene Organic Photovoltaic Cells. *Nat. Commun.* **2013**, *4*, 2867-2877.

(36) Clark, J.; Chang, J. F.; Spano, F. C.; Friend, R. H.; Silva, C. Determining Exciton Bandwidth and Film Microstructure in Polythiophene Films Using Linear Absorption Spectroscopy. *Appl. Phys. Lett.* **2009**, *94*, 117-121.

(37) Spano, F. C.; Silva, C. H- and J-aggregate Behavior in Polymeric Semiconductors. *Annu. Rev. Phys. Chem.* **2014**, *65*, 477-500.

(38) J. Cornil; D. A. dos Santos; X. Crispin; R. Silbey; J. L. Brédas. Influence of Interchain Interactions on the Absorption and Luminescence of Conjugated Oligomers

and Polymers: A Quantum-Chemical Characterization. *J. Am. Chem. Soc.* **1998**, *120*, 1289-1299.

(39) Brown, P. J.; Thomas, D. S.; Köhler, A.; Wilson, J. S.; Kim, J.-S.; Ramsdale, C. M.; Sirringhaus, H.; Friend, R. H. Effect of Interchain Interactions on the Absorption and Emission of Poly (3-hexylthiophene). *Phys. Rev. B* **2003**, *67*, 064203.

(40) Bencheikh, F.; Duché, D.; Ruiz, C. M.; Simon, J. J.; Escoubas, L. Study of Optical Properties and Molecular Aggregation of Conjugated Low Band Gap Copolymers: PTB7 and PTB7-Th. *J. Phys. Chem. C* **2015**, *119*, 24643-24648.

(41) Yi Ho, C. H.; Cao, H.; Lu, Y.; Lau, T. K.; Cheung, S. H.; Li, H. W.; Yin, H.; Chiu, K. L.; Ma, L. K.; et al. Boosting the Photovoltaic Thermal Stability of Fullerene Bulk Heterojunction Solar Cells through Charge Transfer Interactions. *J. Mater. Chem. A* **2017**, *5*, 23662-23666.

(42) Wang, S.; Chang, T. N.; Jiang, X. F.; Pan, Y.; Tan, C. H.; Nesladek, M.; Xu, Q. H.; Loh, K. P. Graphene Oxide–Polythiophene Hybrid with Broad-Band Absorption and Photocatalytic Properties. *J. Phys. Chem. Lett.* **2012**, *3*, 2332-2336.

(43) Hao, X. T.; Mckimmie, L. J.; Smith, T. A. Spatial Fluorescence Inhomogeneities in Light-Emitting Conjugated Polymer Films. *J. Phys. Chem. Lett.* **2011**, *2*, 1520–1525.

(44) Hao, X. T.; Chan, N. Y.; Dunstan, D. E.; Smith, T. A. Conformational Changes and Photophysical Behavior in Poly [2-methoxy-5-(2′-ethyl-hexyloxy)-1, 4-phenylene vinylene] Thin Films Cast under an Electric Field. *J. Phys. Chem. C* **2009**, *113*, 11657-11661.

(45) Yu, G.; Gao, J.; Hummelen, J. C.; Wudl, F.; Heeger, A. J. Polymer Photovoltaic Cells: Enhanced Efficiencies via a Network of Internal Donor-Acceptor Heterojunctions. *Science* **1995**, *270*, 1789-1791.

(46) Li, G.; Zhu, R.; Yang, Y. Polymer Solar Cells. *Nat. Photonics* **2012**, *6*, 153-161.

(47) Rivnay, J.; Mannsfeld, S. C. B.; Miller, C. E.; Salleo, A.; Toney, M. F. Quantitative Determination of Organic Semiconductor Microstructure from the Molecular to Device Scale. *Chem. Rev.* **2012**, *112*, 5488-5519.

(48) Chiu, M. Y.; Jeng, U. S.; Su, C. H.; Liang, K. S.; Wei, K. H. Simultaneous Use of Small‐ and Wide‐Angle X‐ray Techniques to Analyze Nanometerscale Phase Separation in Polymer Heterojunction Solar Cells. *Adv. Mater.* **2008**, *20*, 2573-2578.

(49) Chou, K. W.; Yan, B.; Li, R.; Li, E. Q.; Zhao, K.; Anjum, D. H.; Alvarez, S.; Gassaway, R.; Biocca, A.; et al. Spin‐Cast Bulk Heterojunction Solar Cells: A Dynamical Investigation. *Adv. Mater.* **2013**, *25*, 1923-1929.

(50) Wu, W. R.; Jeng, U. S.; Su, C. J.; Wei, K. H.; Su, M. S. Competition between Fullerene Aggregation and Poly (3-hexylthiophene) Crystallization upon Annealing of Bulk Heterojunction Solar Cells. *ACS Nano* **2011**, *5*, 6233-6243.

(51) Yang, X.; Zheng, F.; Xu, W. L.; Bi, P. Q.; Feng, L.; Liu, J.; Hao, X. T. Improving the Compatibility of Donor Polymers in Efficient Ternary Organic Solar Cells via Post-Additive Soaking Treatment. *ACS Appl. Mater. Inter.* **2016**, *9*, 618-627.

(52) Wu, B.; Wu, Z.; Tam, H. L.; Zhu, F. Contrary Interfacial Exciton Dissociation at Metal/Organic Interface in Regular and Reverse Configuration Organic Solar Cells. *Appl. Phys. Lett.* **2014**, *105*, 103302-103305.

(53) Günes, S.; Neugebauer, H.; Sariciftci, N. S. Conjugated Polymer-Based Organic Solar Cells. *Chem. Rev.* **2007**, *107*, 1324-1338.

(54) Blom, P. W. M.; DeJong, M. J. M.; Munster, M. G. Electric-Field and Temperature Dependence of the Hole Mobility in Poly(p-phenylene vinylene). *Phys. Rev. B* **1997**, *5*, 656-659.

(55) Malliaras, G. G.; Salem, J. R.; Brock, P. J.; Scott, C. Electrical Characteristics and Efficiency of Single-layer Organic Light-emitting Diodes. *Phys. Rev. B* **1998**, *58*, 411-414.

(56) Goh, C.; Kline, R. J.; McGehee, M. D.; Kadnikova, E. N.; Fréchet, J. M. J. Molecular-Weight-Dependent Mobilities in Regioregular Poly(3-hexyl-thiophene) Diodes. *Appl. Phys. Lett.* **2005**, *86*, 122110-122115.

(57) Ray, B.; Lundstrom, M. S.; Alam, M. A. Can Morphology Tailoring Improve the Open Circuit Voltage of Organic Solar Cells? *Appl. Phys. Lett.* **2012**, *100*, 013307-0133010.

(58) Zheng, F.; Yang, X. Y.; Bi, P. Q.; Niu, M. S.; Lv, C. K.; Feng, L.; Qin, W.; Wang, Y. Z.; Hao, X. T.; Ghiggino, K. P. Poly(3-hexylthiophene) Coated Graphene Oxide for Improved Performance of Bulk Heterojunction Polymer Solar Cells. *Org. Electron.* **2017**, *44*, 149-158.

(59) Hoppe, H.; Sariciftci, N. S. Organic Solar Cells: An Overview. *J. Mater. Res.* **2004**, *19*, 1924-1945.

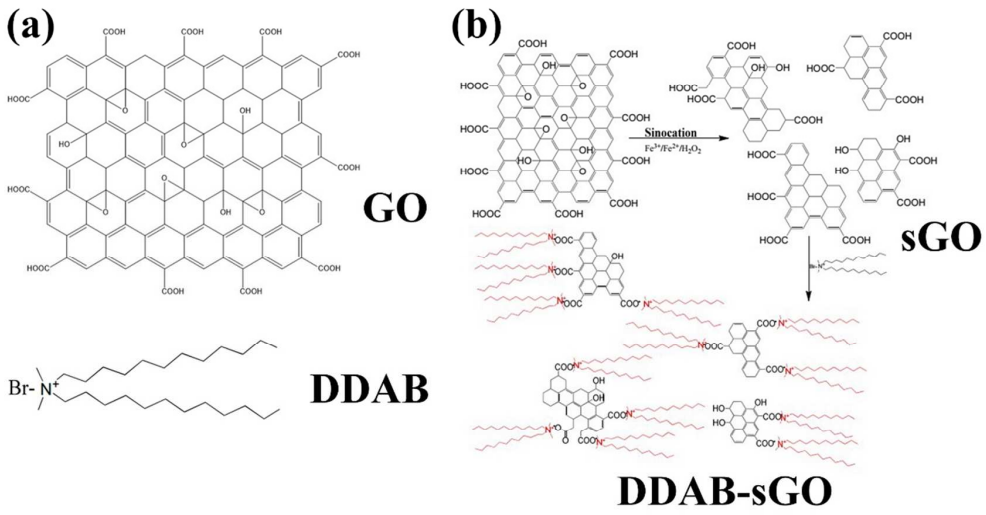

Figure 1. (a) Molecular structures of graphene oxide and DDAB; (b) synthetic procedure for producing DDAB-sGO from GO.

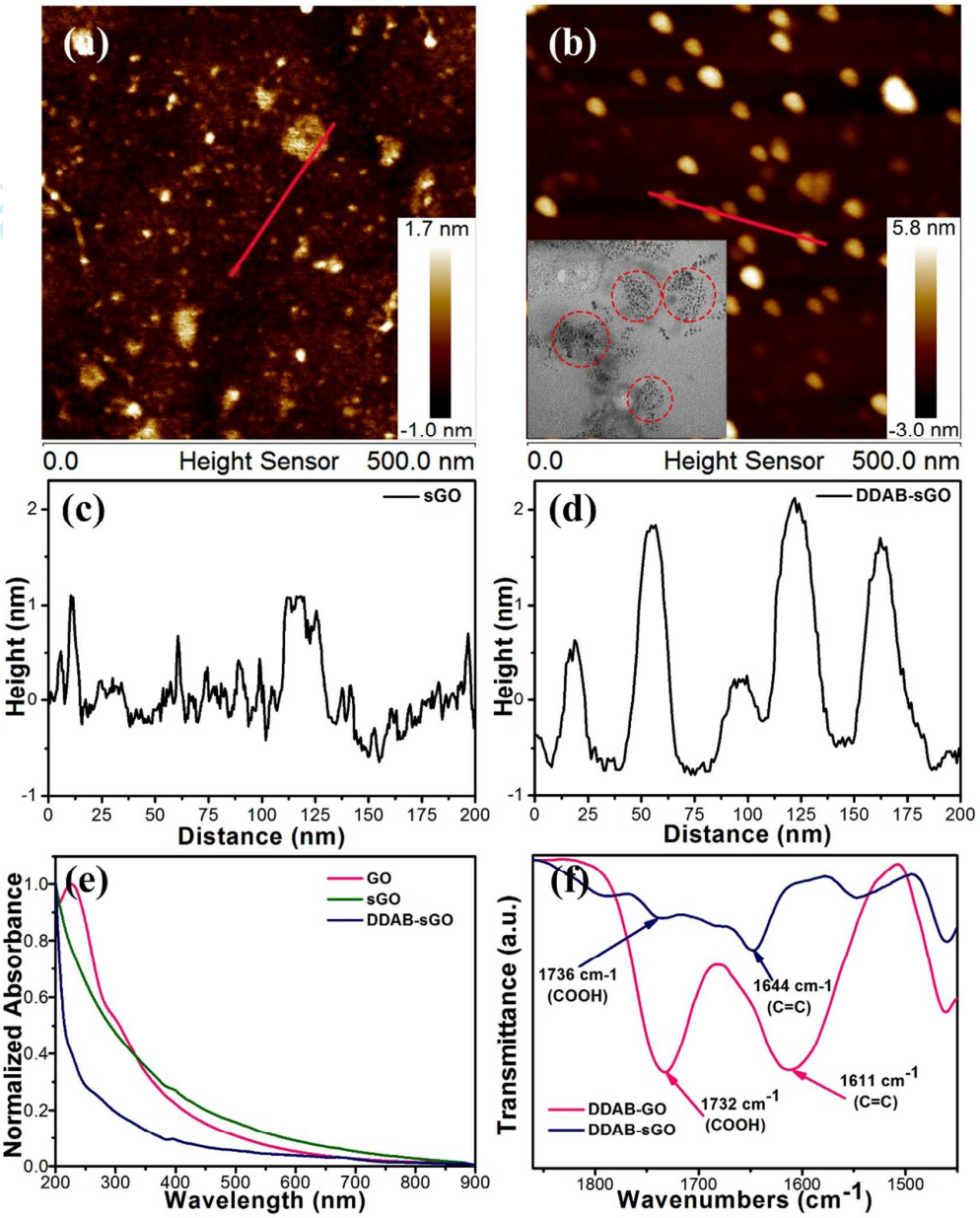

Figure 2. (a, b) AFM images and (c, d) height profiles of sGO and DDAB-sGO (Inset shows TEM image of DDAB-sGO.); (e) Normalized UV-vis absorption spectra of graphene oxide(GO), sGO and DDAB-sGO films; (f) FTIR spectra of DDAB-GO and DDAB-sGO films.

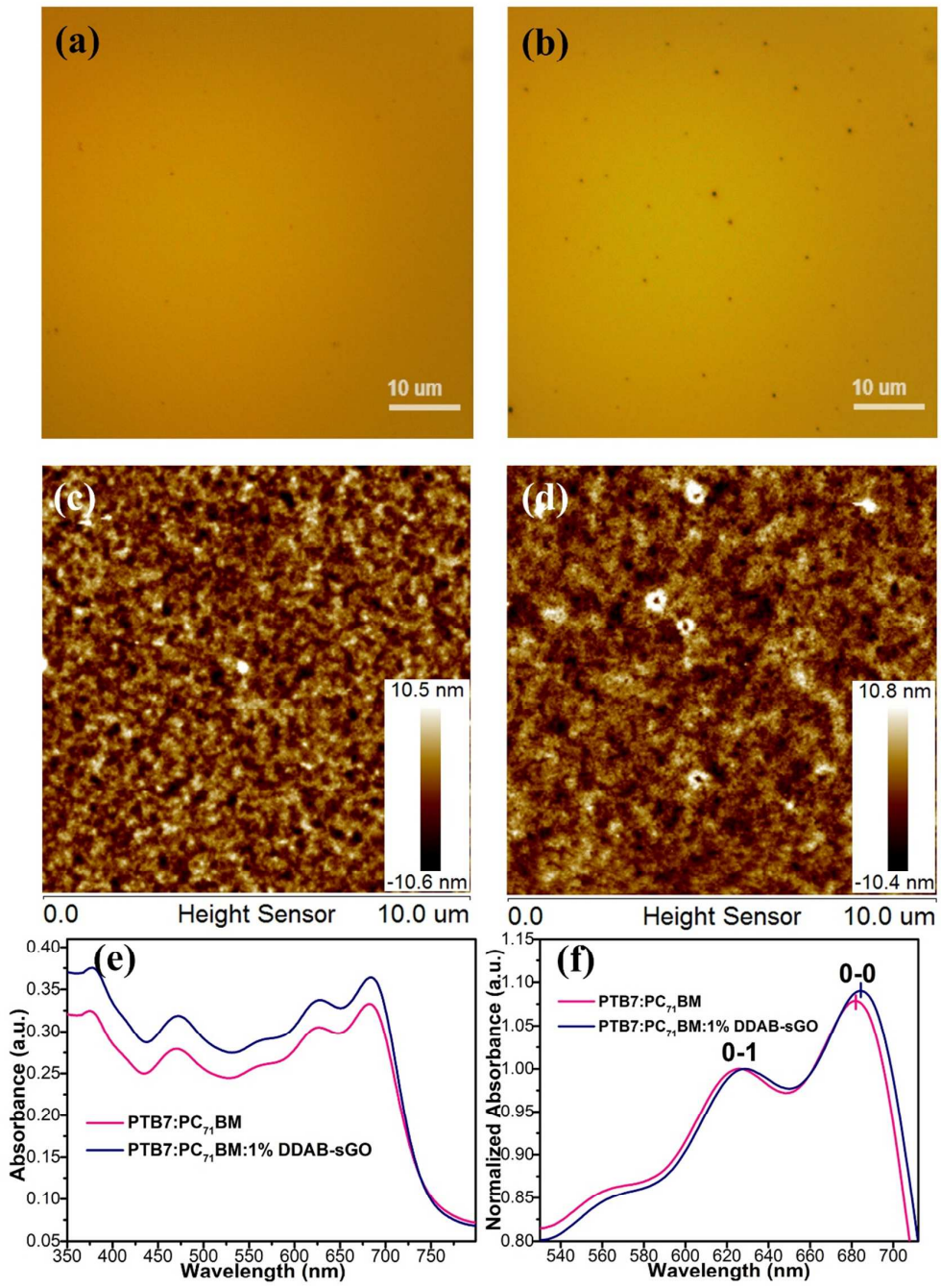

Figure 3. (a, b) Optical microscopy images, (c, d) AFM images, (e) UV-vis spectra and (f) normalized UV-vis spectra (wavelength from 550 nm to 710 nm) of PTB7:$PC_{71}BM$ (left panels) and PTB7:$PC_{71}BM$:1% DDAB-sGO (right panels) films.

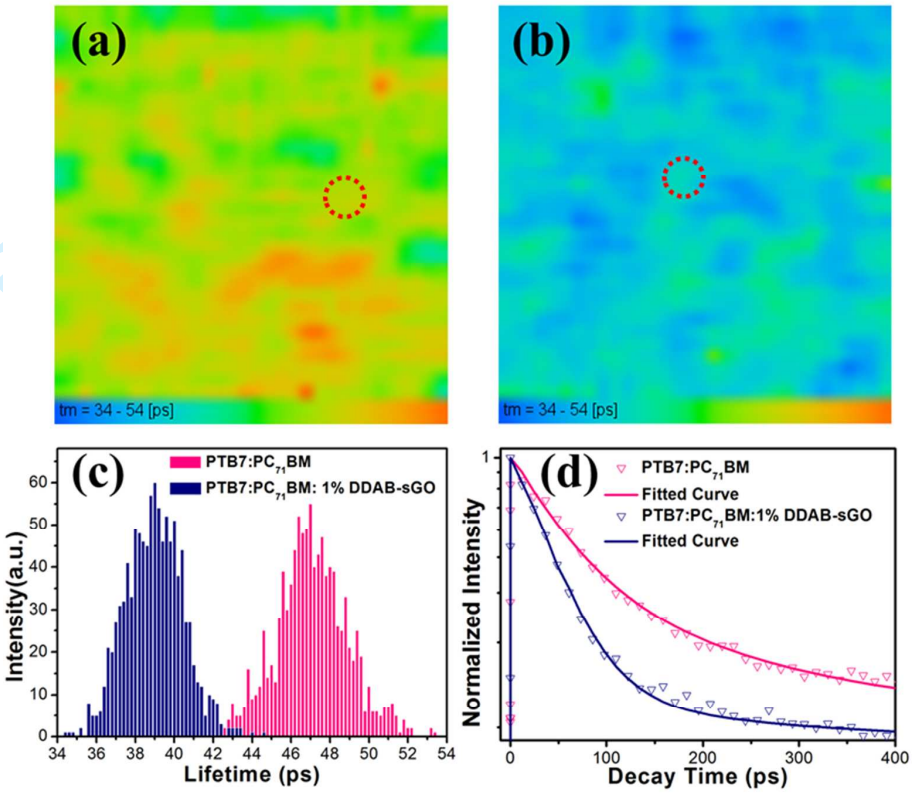

Figure 4. (a, b) 2-D images (20x20μm) with (c) distribution histogram of average fluorescence lifetimes and (d) corresponding fluorescence decay profiles in the selected spots (marked with red dotted circles) of PTB7:$PC_{71}BM$ and PTB7:$PC_{71}BM$:1% DDAB-sGO films. (The intensity values are presented on a logarithmic scale.)

Table 1. Fitting parameters for corresponding fluorescence decay profiles[a] of PTB7:$PC_{71}BM$ and PTB7:$PC_{71}BM$:1% DDAB-sGO films

	A_1 (%)	τ_1 (ps)	A_2 (%)	τ_2 (ps)	t_a (ps)[b]
PTB7:$PC_{71}BM$	89.7	33.6	10.3	177.1	48.3
PTB7:$PC_{71}BM$:1%DDAB-sGO	91.5	25.3	8.5	172.9	37.9

[a]Decay profiles is fitted by $I(t) = A_1 \exp(-\tau_1/t) + A_2 \exp(-\tau_2/t)$.

[b]The average lifetime t_a is calculated from the equation: $t_a = A_1\tau_1 + A_2\tau_2$.

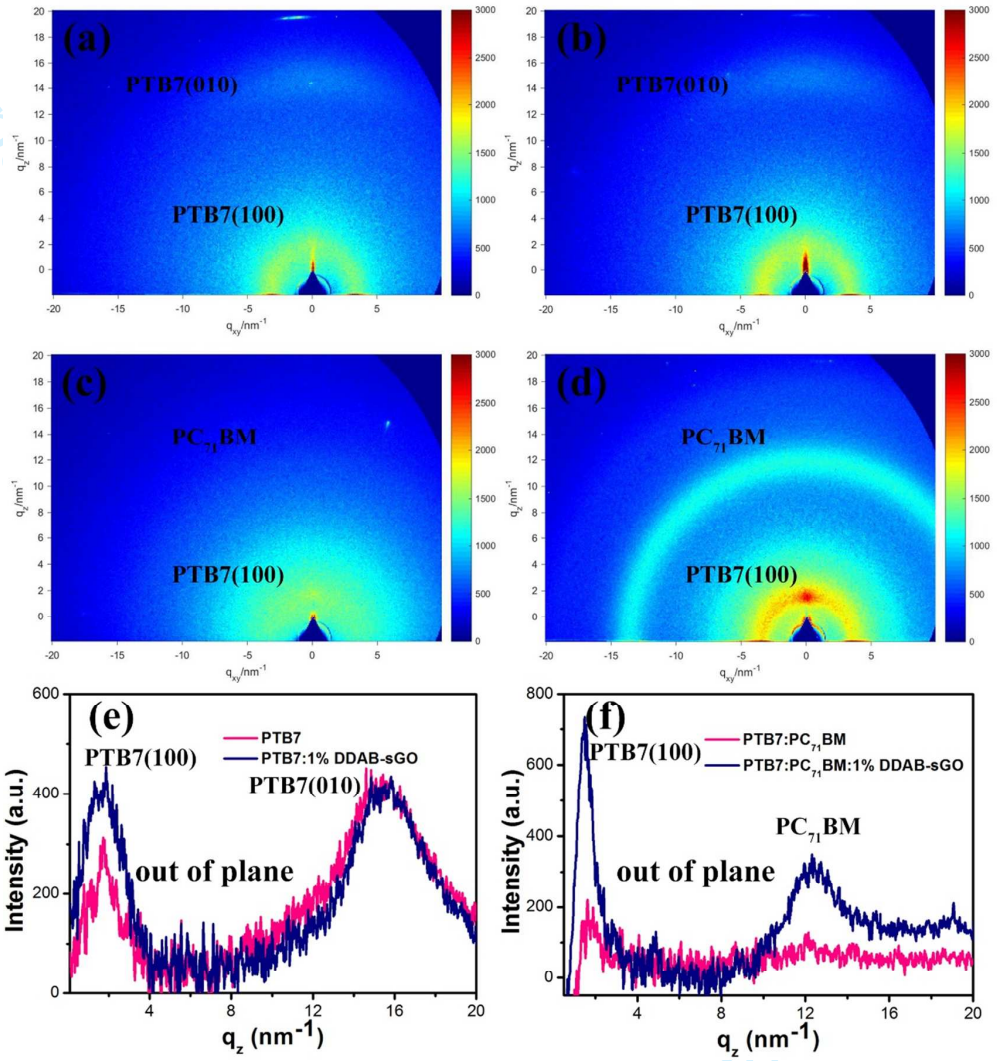

Figure 5. 2-D GIWAXS images of (a) PTB7 and (b) PTB7 with 1% DDAB-sGO films, (c) PTB7:$PC_{71}BM$ and (d) PTB7:$PC_{71}BM$ with 1% DDAB-sGO blend films (the intensity projection along q_z); (e, f) the corresponding intensity projections along the vertical direction.

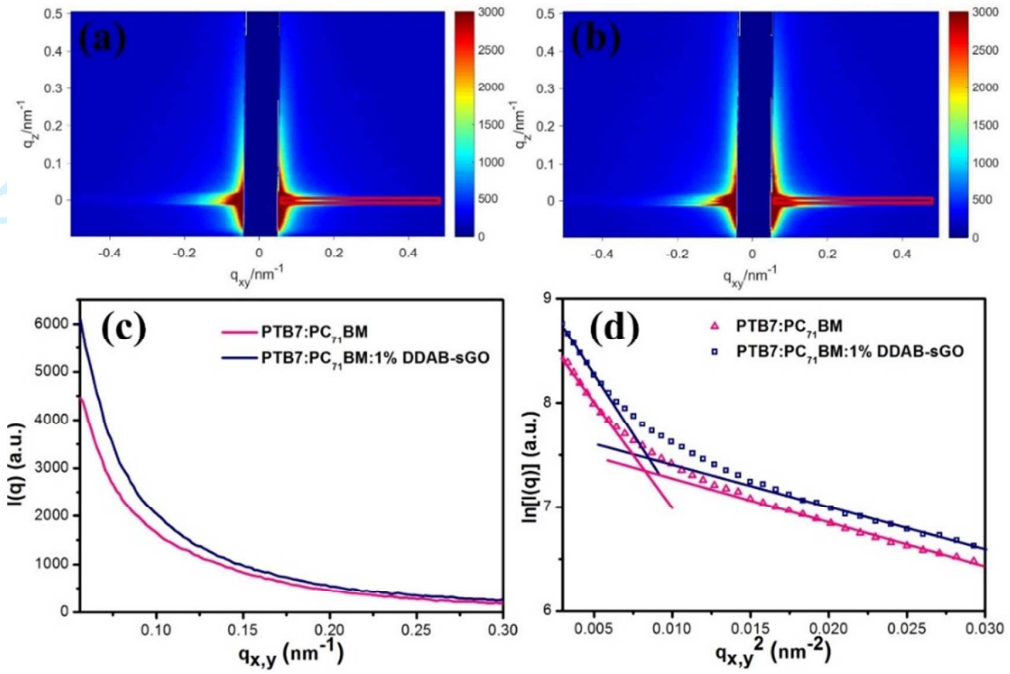

Figure 6. 2-D GISAXS images of (a) PTB7:$PC_{71}BM$ and (b) PTB7:$PC_{71}BM$:1%DDAB-sGO blend films; (c) the corresponding integrated profiles along q_{xy} direction; (d) plots of ln I(q) versus q^2 for the blend films, fitted by the Guinier approximation (straight lines).

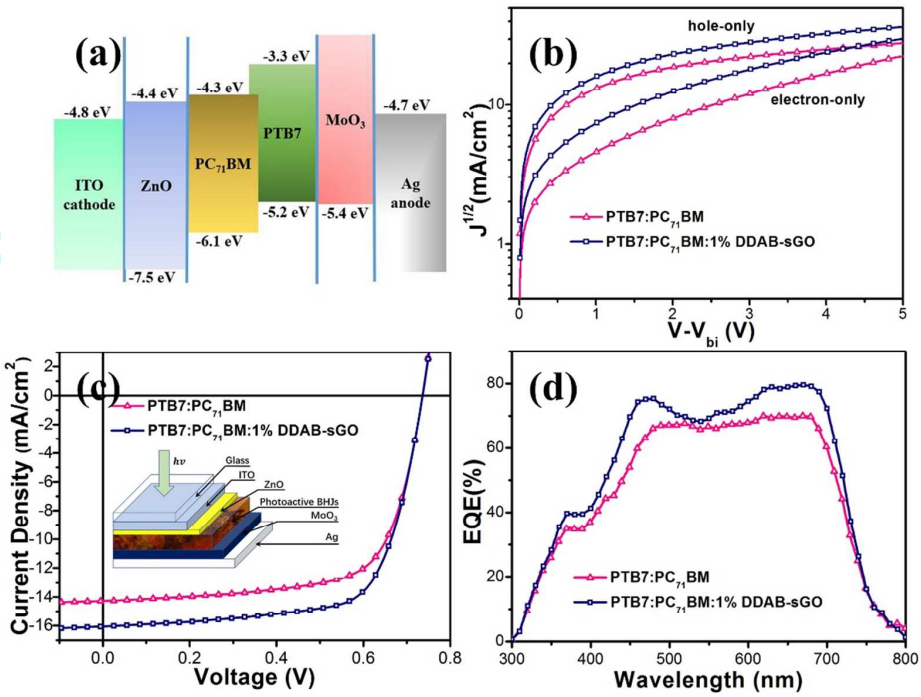

Figure 7. (a) Energy levels diagram, (b) SCLC measurement data for charge carrier mobility, (c) J-V characteristic (Inset shows the schematic diagram of the device structure.) and (d) EQE of solar cells based on PTB7:$PC_{71}BM$ and PTB7:$PC_{71}BM$:1%DDAB-sGO with the best PCE.

Table 2. The performance parameters of PSCs based on PTB7:$PC_{71}BM$ blend films with and without DDAB-sGO incorporation

		V_{OC} (V)	J_{SC} (mA/cm^2)	FF (%)	PCE (%)	μ_h (cm^{2}V^{-1}s^{-1})	μ_e (cm^{2}V^{-1}s^{-1})
PTB7:$PC_{71}BM$	Average[a]	0.74±0.01	14.1±0.2	67±1	7.05±0.05	1.23×10^{-4}	2.14×10^{-4}
	Best PCE[b]	0.74	14.3	67.2	7.1		
PTB7:$PC_{71}BM$:1% DDAB-sGO	Average	0.74±0.01	15.8±0.3	68±2	7.9±0.3	2.63×10^{-4}	4.19×10^{-4}
	Best PCE	0.74	16.1	68.8	8.2		

[a]The "Average" values are obtained by measuring 20 devices.

[b]The "Best PCE" are values of the devices with the highest PCE.

TOC Graphic